Bipolar resistance switching in the fully transparent $BaSnO_3$-based memory device*

Zhang Ting(张 婷)[a)b)], Yin Jiang(殷 江)[a)†], Zhao Gao-Feng(赵高峰)[b)], Zhang Wei-Feng(张伟风)[b)], Xia Yi-Dong(夏奕东)[a)], and Liu Zhi-Guo(刘治国)[a)]

[a)] *National Laboratory of Solid State Microstructure, Nanjing University, Nanjing* 210093, *China*

[b)] *Key Laboratory of Photovoltaic Materials of Henan Province, School of Physics and Electronics, Henan University, Kaifeng* 475004, *China*

(Received 19 October 2013; revised manuscript received 30 January 2014; published online 10 June 2014)

The fully transparent indium–tin-oxide/$BaSnO_3$/F-doped SnO_2 devices that show a stable bipolar resistance switching effect are successfully fabricated. In addition to the transmittance being above 87% for visible light, an initial forming process is unnecessary for the production of transparent memory. Fittings to the current–voltage curves reveal the interfacial conduction in the devices. The first-principles calculation indicates that the oxygen vacancies in cubic $BaSnO_3$ will form the defective energy level below the bottom of conduction band. The field-induced resistance change can be explained based on the change of the interfacial Schottky barrier, due to the migration of oxygen vacancies in the vicinity of the interface. This work presents a candidate material $BaSnO_3$ for the application of resistive random access memory to transparent electronics.

Keywords: transparent resistive random access memory, resistance switching, oxygen vacancy, $BaSnO_3$

PACS: 73.40.–c, 73.40.Rw, 73.50.Fq, 72.20.–i **DOI:** 10.1088/1674-1056/23/8/087304

1. Introduction

Recently, a device composed of an insulating layer sandwiched by two electrodes has been proposed, which showed a reversible electric field-induced resistance switching (RS) effect.[1–11] Based on this effect, a technology for information memory, resistive random access memory (RRAM), can be developed. Up to now, a large variety of materials has been found to show the characteristics of resistance switching, such as the binary oxides,[1,2] the perovskite oxides,[3,4] the solid electrolytes,[5] and P–N junction.[6] To explain the intriguing effect, numerous theoretical models have been proposed. However, the most challenging issue is the lack of an in-depth understanding of the underlying switching mechanism.

Transparent electronics is one of the most important emerging technologies for next-generation electronic systems, and has recently aroused great interest due to its potential to make significant impacts in fields like transparent displays, transparent energy storage, ultraviolet (UV) detectors, and solar cells.[7–9] Since the first demonstration of the fully transparent RRAM (TRRAM) in a structure of ITO/ZnO/ITO by Seo *et al.*,[10] the basic metal–oxide–metal (MOM) structure has been successfully applied to the transparent RRAM (T-RRAM) device by changing the substrate into the glass. In succession, the configurations such as ITO/GaZnO/ITO, GZO/Ga_2O_3/ZnO/Ga_2O_3/GZO,[11] ITO/InGaZnO/ITO,[12] ITO/ZnO:Mg/FTO,[13] and Al:ZnO/Mg:ZnO/Al:ZnO,[14] have been reported. However, up to now, the application to T-RRAM only focuses on the ZnO-based materials. For a universal understanding of the switching mechanism of TRRAM device, it is essential to explore other oxide materials.

Complex ternary transition metal oxides, many of which possess a perovskite structure, have become a major focal point of interest because the majority of these materials possess a host of interesting physical properties with applications in fields ranging from ferroelectricity, ferromagnetism, piezoelectricity, pyroelectricity, and high-temperature superconductivity to optoelectronics.[15] Recently, there has been a considerable amount of interest in electric-field- and/or current-induced nonvolatile resistance switching phenomena in such materials at room temperature.[16–19] Among complex oxides, cubic $BaSnO_3$ has received much attention for its d^{10} electronic configuration.[20,21] The wide band gap (3.4 eV)[22] and high transparence in the visible region make it a potential candidate to realize a fully TRRAM device. In this work, we find that reversible resistive switching occurs repeatedly at room temperature in a $BaSnO_3$ thin film simply layered between the see-through top and bottom electrodes. Therefore, this study may lead to a better understanding of the complex ternary oxides-based memory device for the transparent nonvolatile memory applications and may pave the way for integrated devices with interesting multiple coupled functionalities.

*Project supported by the National Natural Science Foundation of China (Grant Nos. 11174135 and 60976016), the National 973 Project, China (Gant No. 0213117005), the State Key Program for Basic Research of China (Grant No. 2010CB630704), the Science Foundation of Henan Province, China (Grant No. 14A430020), the Science Foundation of Henan University, China (Grant No. SBGJ090503), and China Postdoctoral Science Foundation (Grant No. 2012M511250).

†Corresponding author. E-mail: jyin@nju.edu.cn

© 2014 Chinese Physical Society and IOP Publishing Ltd

2. Experimental procedures

The ceramic targets of $BaSnO_3$ were prepared by a standard solid state reaction method through using $BaCO_3$ and SnO_2 as raw materials. The heterojunctions were fabricated by using the pulsed laser deposition (PLD) technique. Commercial glass capped by a $\sim$ 350-nm-thick F-doped SnO_2 (FTO) layer, which has a transmittance of above 95% and lower sheet resistance (14 $\Omega/\square$), was used as substrate and simultaneously bottom electrode. Firstly, approximate 200-nm-thick $BaSnO_3$ thin films were grown on FTO substrates at 700 °C using a Kr-Fexcimer laser ($\lambda = 248$ nm) with a repetition rate of 5 Hz and a single pulse power of 300 mJ. The deposition was carried out in a pure oxygen atmosphere with a pressure of 20 Pa for 30 s. To measure the electrical properties of the $BaSnO_3$ film, about 50-nm-thick indium–tin-oxide (ITO) top-electrodes with a diameter of 200 μm were deposited by using PLD with a metal shadow mask at 130 °C. The In_2O_3/SnO_2 (9:1) alloy was selected as the target.

The X-ray diffraction (XRD) spectra were collected with a DX-2500 X-ray diffractometer with employing Cu Kα radiation (1.542 Å). The optical transmittance spectra of the films were recorded with a UV–Vis–NIR spectrophotometer (Varian, Cary-5000). The X-ray photoelectron spectroscopy (XPS) images were acquired by using an Axis Ultra spectrometer (Kratos Analytical Ltd) with a monochromatic Al Kα source. Cyclic voltammetry measurements were performed with a CHI600B electrochemical workstation (Chenhua Instruments Inc., China).

The first-principles calculation based on the density functional theory was carried out to study the energy level of oxygen vacancies in cubic $BaSnO_3$. The calculations of the supercells including 40 atoms and containing a single oxygen vacancy were performed by using the Cambridge Sequential Total Energy Package (CASTEP). The energy cutoff for the plane-wave basis was chosen to be 380 eV for describing the electronic wave function, and the Brillouin zone integrations were performed on a well-converged grid of $3\times3\times3$ k-points. The atomic positions and cell parameters were relaxed until the atomic forces and stress tensors were reduced to 0.02 eV/Å and 1 kbar (1 bar = 10^5 Pa) respectively. The total energy converged to 1×10^{-5} eV/atom.

3. Results and discussion

XRD patterns of $BaSnO_3$ films on FTO are shown in Fig. 1. All the diffraction peaks can be indexed to $BaSnO_3$, indicating that the films are of cubic phase and have no impurity. Comparison of XRD patterns between FTO films and $BaSnO_3$/FTO films shows that the peaks shift toward higher angles. Maybe the coherency strains between matrix and substrate domains are responsible for their peak shifts.[23] To quantitatively evaluate the transparency, the optical transmittance of the TRRAM device is investigated (inset of Fig. 1). The average transmittance of the TRRAM device (deducting the substrate's contribution) is approximately 87% in the visible region (400 nm–800 nm in wavelength), indicating the excellent transparency of the RRAM device.

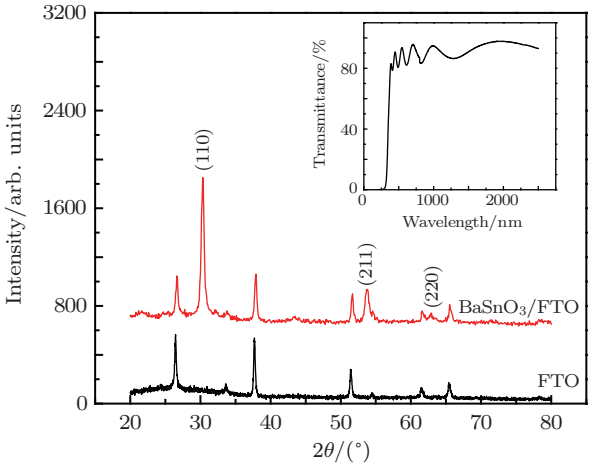


Fig. 1. (color online) XRD patterns of $BaSnO_3$ films deposited on FTO conducting glass. The inset shows the transmittance of TRRAM device.

In order to investigate the dynamic properties of charge carriers in the heterojunctions, the measurements of the electrical switching behaviors are performed. As shown in the inset of Fig. 2(a), all the electrochemical measurements were carried out by using a three-electrode system with FTO serving as the reference electrode and counter electrode, and ITO as the working electrode. The current–voltage (I–V) characteristic of ITO/$BaSnO_3$/FTO under the voltage sweep $0 \rightarrow V_{max} \rightarrow 0 \rightarrow -V_{max} \rightarrow 0$ is shown in Fig. 2. Here, the positive bias is defined as an electric current flowing from ITO to FTO. Figure 2(a) displays the 50 consecutive measurements of the hysteretic I–V characteristic between +5 V and −5 V at a scan rate of 0.3 V/s. It can be seen that all the curves exhibit nonlinear and asymmetric behaviors, indicating a good retention characteristic and a bipolar resistance switching behavior of the device. As shown in the figure, the current increases nonlinearly with the applied voltage increasing from 0 V to $+V_{max}$ without forming steps, displaying a low resistance state (LRS). When the bias voltage is scanned from $+V_{max}$ to $-V_{max}$, a lower current is observed, displaying a high resistance state (HRS). When the polarity of the bias is changed, the device switches from HRS to the LRS. The quasi-static measurements are performed to investigate whether the switching voltage is affected by the scanning rate. Figure 2(b) presents the I–V loops measured with different scanning rates. It is observed that the hysteresis window enlarges with increasing scanning rate, and the self-accelerated thermal dissolution model could give it a rational explanation.[24] Since the process is thermally driven, the kinetics will depend on the voltage and current,

which respectively control the Joule power and the temperature in the film. The initial thermal dissolution of the film enhances temperature and further dissolution, resulting in a self-accelerated dissolution mechanism. In the case of higher sweep rate, more charges are supplied, and hence, a lower resistance could grow. As a result, the current increases with increasing the voltage ramp speed. This means that for practical memory operation in the high sweep rate regime, current will be much larger than that in the quasi-static case, which is most typically used for the basic characterization of RRAM devices.

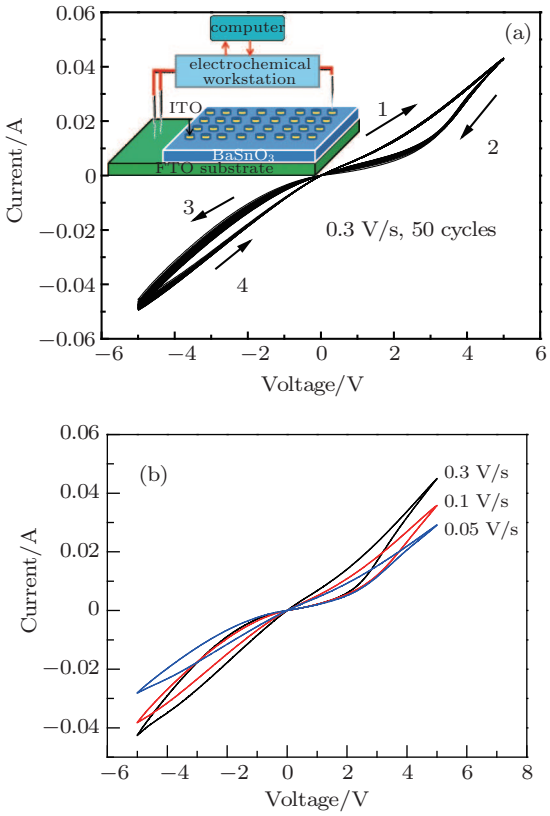


Fig. 2. (color online) (a) *I*–*V* curves for 50 consecutive measurements performed with a 0.3-V/s scanning rate at room temperature. The inset shows the schematic drawing of ITO/$BaSnO_3$/FTO structure and electrical measurement system. (b) *I*–*V* characteristics of ITO/$BaSnO_3$/FTO sandwich structure with different scanning rates.

To acquire further knowledge about the ER effect in the ITO/$BaSnO_3$/FTO system, we carefully study the *I*–*V* dependence. As shown in Fig. 3(a), the *I*–*V* curve measurements with V_{max} are performed at a scanning rate of 0.3 V/s. The *I*–*V* loop appears and develops with the increase of bias voltage V_{max}. The reason for this might be that the increased V_{max} would significantly reduce the height of the effective Schottky-like barrier and narrow the thickness of the depletion layer, resulting in a smaller LRS and therefore a more prominent hysteresis. A similar phenomenon has been observed in Ag/TiO_2/Nb:$SrTiO_3$/In device.[25] Therefore, a multi-level memory can be achieved by changing the amplitude of the voltage. To investigate the different origins of the switching behaviors, we also carry out nonlinear fittings to the transport characteristics. Figure 3(b) shows the log*I*–log*V* plot linear fitting results for each conduction state. Generally, on-states exhibit Ohmic behaviors with slopes close to 1. The Ohmic conduction dominates the transport behavior when the density of injected carriers in the film is lower than that of the thermally generated ones. For the near-zero voltage region, most of the carriers are trapped at the trap sites and hop to neighboring sites under the action of voltage applied. It should be noted that the trapped carriers are not easily detrapped fully with increasing the positive bias or even with negative bias applied to the top electrode. A much higher density of carriers traps (probably oxygen vacancies) can cause the resistance to change by trapping or detrapping the carriers. This may be the reason for the change of current even under the same

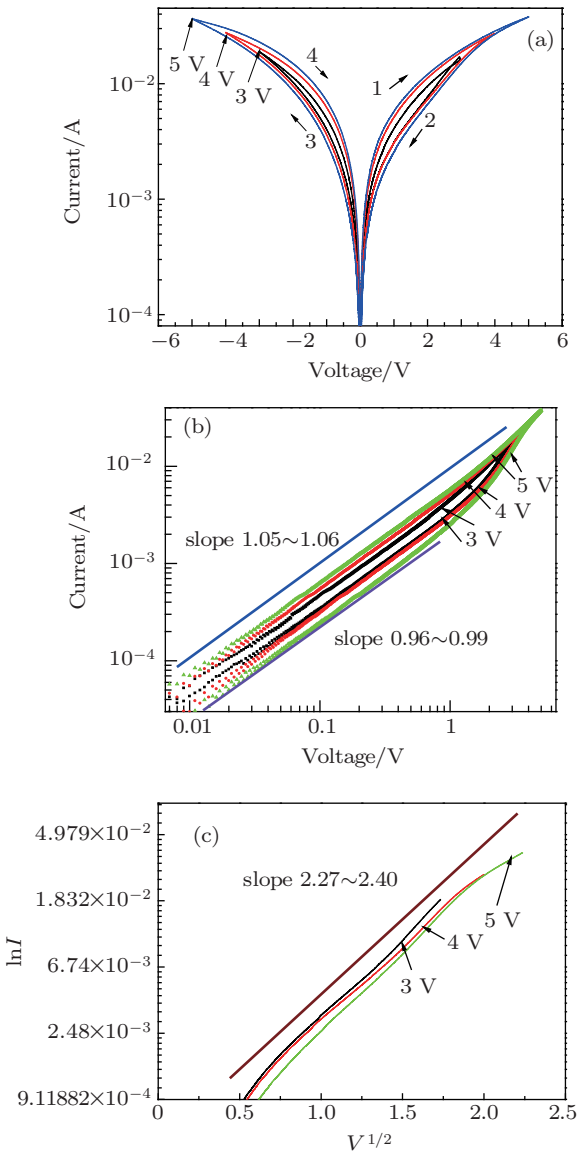


Fig. 3. (color online) (a) *I*–*V* characteristics of $BaSnO_3$-based sandwich structure memory devices. (b) *I*–*V* characteristics of the ITO/$BaSnO_3$/FTO device in log–log scale for the positive voltage regions. (c) The Schottky emission at HRS. The different values of V_{max} are all used in the cases of (a), (b), and (c).

test conditions. With the increase of bias voltage, HRS exhibits first an $I \propto V$ then a $\ln I \propto V^{0.5}$ relationship as shown in Figs. 3(b) and 3(c). This current increasing exponentially with the square root of the applied bias could be considered to be due to Schottky conduction. The Schottky mechanism is the metal/insulator interfacial effect, which arises from the lowering of the Schottky barrier with electric fields. The Schottky equation is expressed as follows:[26]

$$I \propto T^2 \exp\left[\frac{e\sqrt{(eV)/(4\pi\varepsilon_i\varepsilon_0 d)}}{kT}\right], \quad (1)$$

where I is the current, e is the electronic charge, ε_0 is the permittivity of free space, ε_i is the dielectric constant, V is the applied voltage, d is the thickness of a film, and k is the Boltzmann's constant.

As is well known, oxide films prepared by using pulsed laser deposition in an oxygen-deficient chamber contain a large number of oxygen vacancies, and those defects are deemed to play an important role in the resistance hysteresis. For a better understanding of the influence of defects on the electric property of $BaSnO_3$ sample, the XPS profiles for O 1s core level are measured. The presence of the non-lattice oxygen ions in the film can be supported by XPS analysis of the $BaSnO_3$ thin film as shown in Fig. 4. The XPS peaks for O 1s core level can be consistently fitted by three different near-Gaussian subpeaks centered at 529.2, 530.9, and 532.0 eV respectively. The first one can be assigned to the perovskite structure of $BaSnO_3$, the second one at 530.9 eV to molecular O_2 species, and the last one at about 532.0 eV to oxygen in OH^-.[27] The XPS binding energies of the film are affected by the presence of the non-lattice oxygen, which implies the existence of oxygen vacancies (V_O).[28,29] Due to the fact that the film thickness is far greater than the detecting depth of instrument, the non-lattice oxygen cannot be derived from FTO substrate. The presence of the non-lattice oxygen ions are likely to play an important role in changing the resistance. Kim *et al*. revealed that a considerable number of the non-lattice oxygen ions exist in GaZnO film, and these non-lattice oxygen ions allow the forming operation to be omitted.[1] Sufficient non-lattice oxygen ions in $BaSnO_3$ film allows our TRRAM to be operated without a forming process. Oxygen vacancy is actually caused by non-lattice oxygen ions, and the number of oxygen vacancies is proportional to the ratio of non-lattice oxygen.[30] To analyze the potential role and the mechanism for lattice strain in tuning the reactivity of $BaSnO_3$ with oxygen ions, the total density of states (TDOS) and partial density of states (PDOS) of cubic $BaSnO_3$ supercells without and with oxygen vacancy are plotted in Fig. 5. As expected in the case of $BaSnO_3$, the top of the valence band is dominated by the contribution from the O 2p orbital, while the bottom of the conduction band is predominantly due to the contribution from Sn 5s orbitals. Ba 6s orbitals make a small contribution to the lower region of the conduction band. It is well known that in perovskite oxide, the oxygen ions migrate much more easily than other cations, and the ionization of the oxygen vacancies could create the conduction electrons,

$$O_O \Leftrightarrow V_O + (1/2)O_2, \quad (2)$$

$$V_O \Leftrightarrow V_{\dot{O}} + e', \quad (3)$$

$$V_{\dot{O}} \Leftrightarrow V_{\ddot{O}} + e', \quad (4)$$

where the notations defined by Kröger and Vink are adopted; $V_{\dot{O}}$ and $V_{\ddot{O}}$ represent the oxygen vacancies carrying one and two positive charges respectively.[31] Our calculation indicates that the oxygen vacancies in cubic $BaSnO_3$ will form a defective energy level below the bottom of conduction band, and reduce the band gap.

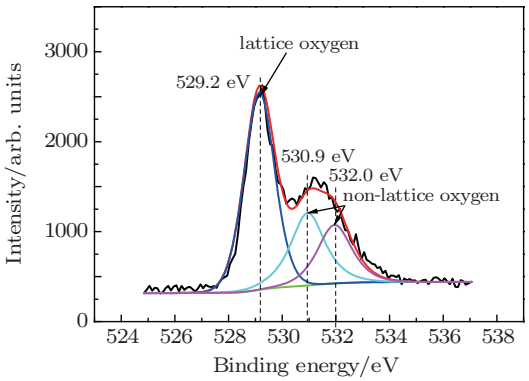


Fig. 4. (color online) XPS characteristics of O 1s for the $BaSnO_3$ films deposited on FTO substrates.

It is well known that electrode selection is important for RRAM performance. These differences in the work function and conductivity between the electrodes and the function layer can modify the Schottky barrier height at each interface,[1] resulting in asymmetric I–V switching curves. In a very recent report, different RS mechanisms of NiO thin films were explored by changing the bottom electrodes; Pt and $SrRuO_3$ electrodes led to filamentary conduction and formation of interfacial Schottky barrier respectively.[26] Peng *et al*. reported that Mn-doped ZnO thin films grown on Pt and Si show unipolar and bipolar RS behaviors respectively. They explained the unipolar RS by filamentary conduction and the bipolar RS by interfacial effect.[32] In the asymmetric structure ITO/$BaSnO_3$/FTO device, the bipolar RS behavior is consistent with previously reported results about the interfacial effects,[26,33] where the migration of oxygen vacancies in the vicinity of the interface drives RS in various heterojunctions.[34] It was observed that the O/Ni ratio is higher near the interface of NiO/ITO because the ITO bottom electrode serves as a reservoir of oxygen ions.[35] So we can consider that the FTO bottom electrode may act as an oxygen supplier. Bipolar switching of ITO/BaSnO3/FTO may be related to the change in the height or width of Schottky barrier,

due to the migration of oxygen vacancies in the vicinity of the interface. In an n-type oxide semiconductor, oxygen vacancies are considered to be effective donors. A positive (or negative) polarity sweep traps (or de-traps) oxygen vacancies at the FTO/$BaSnO_3$ interface. The addition (or reduction) in oxygen vacancies at the interfaces may cause the depletion layer to become wider (or narrower) in $BaSnO_3$, resulting in the increasing (or decreasing) of Schottky barrier and the switching of the contact resistance from ON (or OFF) to the OFF (or ON) state. Although the detailed investigations on the hysteretic current–voltage characteristics, such as symmetric electrodes structure, area-dependence,..., were not performed in our work, it can still be suggested that the migration of oxygen vacancies in the vicinity of the interface drives the RS effect.

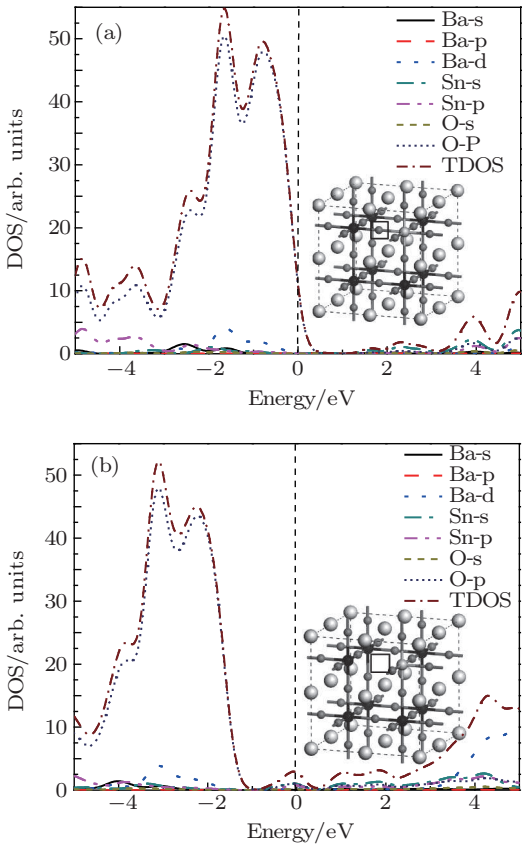


Fig. 5. (color online) DOS for $BaSnO_3$ supercells including 40 atoms without oxygen vacancy (a) and with an oxygen vacancy (b). The inset shows the schematic picture of the oxygen vacancy chain system in 2×2×2 supercell of cubic $BaSnO_3$. The red (small gray ball) represents oxygen, the green (big gray ball) represents Ba, and the gray (black ball) represents Sn.

In order to evaluate the potential for application in TRRAM, the retention tests are performed for ITO/$BaSnO_3$/FTO memory device, and the results are shown in Fig. 6(a). The retention properties over a period of 2×10^4 s for two states triggered by 2.5 V/1 s and −2.5 V/1 s pulses remain almost unchanged. Figure 6(b) demonstrates the multilevel resistive switching of $BaSnO_3$ film device. Different high resistance states are obtained by applying voltage pulses of 3, 3.5, and 4 V/0.002 s, and the changed low resistance states are also observed by applying pulse voltages of −3, −3.5, and −4 V/0.002 s. Over 1×10^4 switching cycles, two states triggered respectively by the positive and the negative electric pulses become negligibly degraded. This multilevel resistive switching feature can be used as the high-density storage. These results indicate that TRRAM is highly promising as a future nonvolatile memory device.

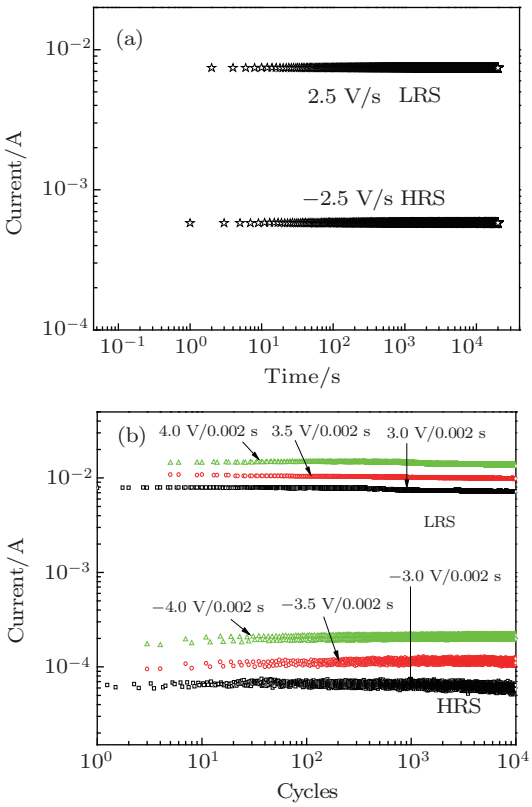


Fig. 6. (color online) Plots of (a) retention and (b) endurance properties characterized at room temperature.

4. Conclusions

In this paper, fully transparent RRAM devices based on an ITO/$BaSnO_3$/FTO sandwich structure are fabricated by using PLD technique. The TRRAM devices exhibit excellent transmittance of more than 87% in the visible region. Without an initial forming process, the TRRAM shows a reasonable bipolar resistive switching behavior. Bipolar switching may be related with the change in the height or width of Schottky barrier induced by applying voltage, resulting in Ohmic on-state I–V, Schottky off-state I–V. The XPS analyses reveal that a considerable number of the non-lattice oxygen ions exist in $BaSnO_3$ film, and these non-lattice oxygen ions allow the forming operation to be omitted. The first-principles calculations suggest that the oxygen vacancies in cubic $BaSnO_3$ will form defective energy level below the bottom of the conduction band, thereby reducing the band gap. The resistance variation in the film in the resistive switching process should

be attributed to the trapping or de-trapping of oxygen vacancies at the Schottky-type interface. With the excellent retention and endurance properties, the fully transparent memory devices could pave the way for transparent electronics and other future applications, including flexible electronic papers and smart window.

References

[1] Kim A, Song K, Kim Y and Moon J 2011 *ACS Appl. Mater. Interfaces* **3** 4525
[2] Bae J, Hwang I, Jeong Y, Kang S, Hong S, Son J, Choi J, Kim J, Park J, Seong M, Jia Q and Park H B 2012 *Appl. Phys. Lett.* **100** 062902
[3] Zhang T, Ding L H and Zhang W F 2012 *Chin. Phys. B* **21** 047301
[4] Zhang T, Bai Y, Jia C H and Zhang W F 2012 *Chin. Phys. B* **21** 107304
[5] Huang J Q, Shi L P, Yeo E G, Yi K J and Zhao R 2012 *IEEE Electron Dev. Lett.* **33** 98
[6] Kim K M, Song S J, Kim G H, Seok J Y, Lee M H, Yoon J H, Park J and Hwang C S 2011 *Adv. Funct. Mater.* **21** 1587
[7] Shen G, Xu J, Wang X, Huang H and Chen D 2011 *Adv. Mater.* **23** 771
[8] Kawazoe H, Yasukawa M, Hyodo H, Kurita M, Yanagi H and Hosono H 1997 *Nature* **389** 939
[9] Wagner J F 2003 *Science* **300** 1245
[10] Seo J W, Park J W, Lim K S, Yang J H and Kang S J 2008 *Appl. Phys. Lett.* **93** 223505
[11] Zheng K, Sun X W, Zhao J L, Wang Y, Yu H Y, Demir H V and Teo K L 2011 *IEEE Electron Dev. Lett.* **32** 797
[12] Chen M C, Chang T C, Huang S Y, Chen S C, Hu C W, Tsai C T and Sze S M 2010 *Electrochem. Solid-State Lett.* **13** H191
[13] Shi L, Shang D, Sun J and Shen B 2009 *Appl. Phys. Exp.* **2** 101602
[14] Cao X, Li X, Gao X, Liu X, Yang C, Yang R and Jin P 2011 *J. Phys. D: Appl. Phys.* **44** 255104
[15] Zhou H J, MaoY B and Wong S S 2007 *Chem. Mater.* **19** 5238
[16] Liu S Q, Wu N J and Ignatiev A 2000 *Appl. Phys. Lett.* **76** 2749
[17] Fujii T and Kawasaki M 2007 *Phys. Rev. B* **75** 165101
[18] Peng H Y and Wu T 2009 *Appl. Phys. Lett.* **95** 152106
[19] Wu S X, Peng H and Wu T 2011 *Appl. Phys. Lett.* **98** 093503
[20] Yuan Y P, Lü J, Jiang X J, Li Z S, Yu T, Zou Z G and Ye J H 2007 *Appl. Phys. Lett.* **91** 094107
[21] Borse P H, Joshi U A, Ji S M, Jang J S, Lee J S, Jeong E D and Kim H G 2007 *Appl. Phys. Lett.* **90** 034103
[22] Bouhemadou A and Haddadi K 2010 *Solid State Sci.* **12** 630
[23] Mayrhofer P H, Hörling A, Karlsson L, Sjölén J, Larsson T, Mitterer C and Hultman L 2003 *Appl. Phys. Lett.* **83** 2049
[24] Russo U, Ielmini D, Cagli C and Lacaita A L 2009 *IEEE Trans. Electron Dev.* **56** 193
[25] Zhu Y D, Li M Y, Zhou H, Hu Z Q, Liu X L, Fang X L, Sebo B, Fang G J and Zhao X Z 2012 *J. Phys. D: Appl. Phys.* **45** 375303
[26] Choi J S, Kim J S, Hwang I R, Hong S H, Jeon S H, Kang S O, Park B H, Kim D C, Lee M J and Seo S 2009 *Appl. Phys. Lett.* **95** 022109
[27] Manorama S V, Gopal Reddy C V and Rao V J 2001 *Appl. Surf. Sci.* **174** 93
[28] Huang J J, Kuo C W, Chang W C and Hou T H 2010 *Appl. Phys. Lett.* **96** 262901
[29] Biju K P, Liu X J, Bourim E M, Kim I, Jung S, Siddik M, Lee J and Hwang H 2010 *J. Phys. D: Appl. Phys.* **43** 495104
[30] Shin J, Insung Kim I, Biju K P, Jo M, Park J, Lee J, Jung S, Lee W, Kim S, Park S and Hwang H 2011 *J. Appl. Phys.* **109** 033712
[31] Xia Y D, Liu Z G, Wang Y, Shi L, Chen L, Yin J and Meng X K 2007 *Appl. Phys. Lett.* **91** 102904
[32] Peng H Y, Li G P, Ye J Y, Wei Z P, Zhang Z, Wang D D, Xing G Z and Wu T 2010 *Appl. Phys. Lett.* **96** 192113
[33] Harada T, Ohkubo I, Tsubouchi K, Kumigashira H, Ohnishi T, Lippmaa M, Matsumoto Y, Koinuma H and Oshima M 2008 *Appl. Phys. Lett.* **92** 222113
[34] Sawa A 2008 *Mater. Today* **11** 28
[35] Peng H Y, Li Y F, Lin W N, Wang Y Z, Gao X Y and Wu T 2012 *Sci. Rep.* **2** 442